

Actuation Compensation for Flexible Surgical Snake-like Robots with Redundant Remote Actuation

Kai Xu, Nabil Simaan

ARMA – Advanced Robotics and Mechanism Applications laboratory
Department of Mechanical Engineering, Columbia University
New York, NY 10027, USA
{kx2102, ns2236}@columbia.edu

Abstract – This paper presents two actuation compensation methods for a snake-like robot implementing multi flexible backbones and actuation redundancy. This snake-like robot is designed for distal dexterity enhancement in MIS surgery of the throat. Actuation compensation is required to account for the flexibility of the actuation lines that connect this snake-like robot with its remote actuation units. The paper presents both a naive model-based compensation approach and a combined model-based recursive linear-estimation approach that uses data gathered from external measurements of the snake-like unit configuration such as vision. The kinematic and static model of this multi-backbone snake-like unit is reviewed and a simplified redundancy resolution is implemented in the error compensation model. The results show that the performance of the snake-like unit is significantly improved when compensation is implemented. The combined model-based recursive linear estimation method showed 1° accuracy in path tracking. Finally, an updated Jacobian that accounts for the required compensation is presented. All the work done here strides the crucial step towards a successful clinical task such as suturing in the throat.

Index Terms – Flexible stem, snake robots, surgical assistant, linear estimation, actuation redundancy.

I. INTRODUCTION

Distal dexterity enhancement in Minimally Invasive Surgery (MIS) is a key enabler for complex tasks in confined spaces [1-3]. For this reason many works focused on various ways to overcome the dexterity constraints introduced by the “fulcrum effect” in MIS. These works included planar and spatial linkages [4, 5], parallel wrists [6, 7], serial articulated wrists [8-10], and more recently snake-like devices [4, 10-16] to allow surgeons to control the position and orientation of surgical tools. Distal dexterity improvement was investigated in robotic systems for laparoscopy [9, 17], arthroscopy [12], gastro-intestinal surgery [11, 16], neurosurgery [14], fetal surgery [13], and ENT surgery (e.g. [18], [19]). The actuation methods for these devices included wire actuation [9, 13, 14], SMA actuation [12], mechanical actuation through linkages [5], gear transmission [4], and our recent design which implements push-pull actuation by using flexible super-elastic members [3, 20, 21].

In many applications in MIS, the actuators are remotely located to provide MRI compatibility or because of space limitations. The classical use of wire-actuation and articulated

wrists suffers from limited reliability of the wires, backlash and pre-tensioning problems. Inspired by the works of [22, 23] using a single flexible backbone, a miniature $\varnothing 4.2$ mm snake-like device for MIS of the throat and upper airways is developed, Fig 1. This snake-like unit overcomes some of the problems of wire actuated wrists by using multiple super-elastic NiTi backbones for actuation and provides the structural rigidity required to faithfully manipulate a surgical tool in tele-manipulation.

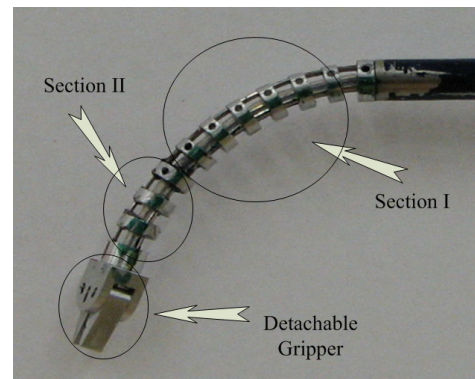


Fig 1. A detachable gripper and the $\varnothing 4.2$ mm two-section snake-like device

While the introduction of flexible backbones eliminates significant backlash problems, promotes miniaturization and allows for actuation redundancy in push-pull mode, it also introduces modeling problems due to the flexibility and friction in the actuation lines. The actuation lines connecting the actuation unit and the snake-like unit may pass through a rigid tube (e.g. in our case [3]) or a flexible stem (e.g. [18]). Regardless, of the method used, it is necessary to compensate for extension in the actuation lines due to friction and to the actuation forces required to bend the flexible snake-like unit. This compensation is important for faithful control in master-slave mode and also to provide a method to account for varying loads on the snake-like unit.

Inverse kinematics compensation for flexible robots has been widely studied by [24-26]. Svinin [25] applied iterative process to find compensation of the deflection. Meggiolaro [24] used linear combinations of columns of the system identification Jacobian matrix to eliminate parameter redundancy for a precise compensation. Combining their ideas on the serial robots, we adopt a recursive estimation procedure

to update the system model to compensate for mechanical errors.

In section II, we present the structure, the kinematic and static modeling of the snake-like device, and we point out the sources of the error. In section III we propose a model-based compensation to account for the flexibility of the actuation lines. In section IV, the experimental results are presented, using a naive compensation scheme that does not account for backlash and any other mechanical errors in the actuation unit. In section V, we apply a combined model-based least-squares recursive linear estimation algorithm that relies on external measurements of the snake configuration (e.g. through vision) to improve the estimates of friction, load, and some parasitic backlash that may be present in the actuation lines, to finally achieve precise trajectory tracking. Section VI presents the experimental results that show significant improvement in trajectory tracking accuracy.

II. THE SNAKE-LIKE UNIT

Figure 2 shows the Distal Dexterity Unit (DDU) composed from the snake-like unit of Fig. 1 and a parallel manipulation unit. The snake-like unit provides the gross motion capabilities while the parallel manipulation unit provides high accuracy localized 3 DoF motion at the tip of the DDU. The snake-like unit has four super-elastic NiTi tubes as its backbones. One primary backbone is located at the center and is attached to all the disks of the snake-like unit. Three identical secondary backbones are equidistant from each other and from the primary backbone. The secondary backbones are only attached to the end disk and can slide in appropriately toleranced holes in the spacer disks and the base disk. Each secondary backbone is actuated in push-pull mode by an actuation unit through a 480 mm long DDU holder and a channel in the snake cone, Fig. 3. Two DOF motion of the snake-like unit is achieved through simultaneous actuation of the secondary backbones. Although we have proved this kind of novel structure is theoretically superior to the wire-driven snake-like robots in supporting miniaturization and eliminating backlash [21], it presents difficulties in modelling and control due to the flexibility of the actuation elements.

The generalized solution for the inverse kinematics of hyper redundant robots was given by [27, 28]. In this case, the kinematics of continuous backbone snake-like robots was addressed by [3, 22, 23]. The nomenclature used in this paper is hereby summarized, Fig. 4.

Three coordinates systems are defined: the Base Disk Coordinate System $\{\hat{x}_b, \hat{y}_b, \hat{z}_b\}$, the Snake Plane Coordinate System $\{\hat{x}_1, \hat{y}_1, \hat{z}_1\}$, and the End Disk Coordinate System $\{\hat{x}_e, \hat{y}_e, \hat{z}_e\}$. The symbols used are defined as below:

- i - Index of the secondary backbones, $i = 1, 2, 3$.
- s - Arc-length parameter of the primary backbone
- L, L_i - Length of the primary and the i^{th} secondary backbone measured from the base disk to the end disk
- $q_i = L_i - L$ - Joint displacement of the i^{th} secondary backbone

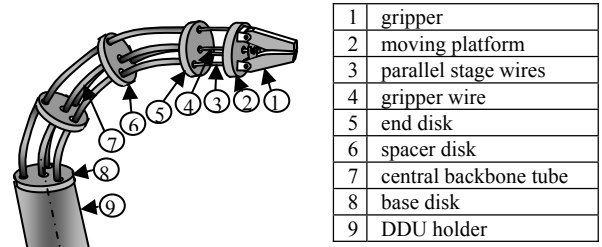


Fig. 2. The Distal Dexterity Unit (DDU) composed from a parallel manipulation unit and a snake-like unit.

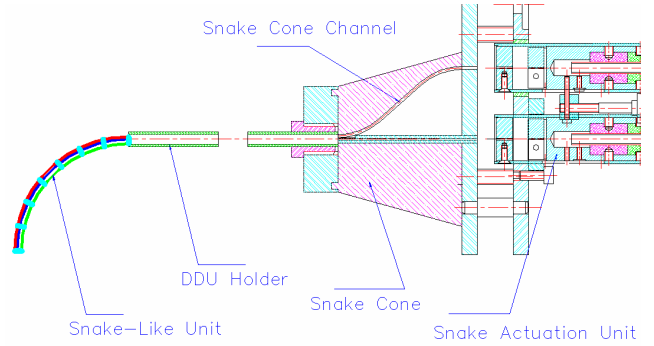


Fig. 3. A schematic of the actuation unit and the snake-like unit.

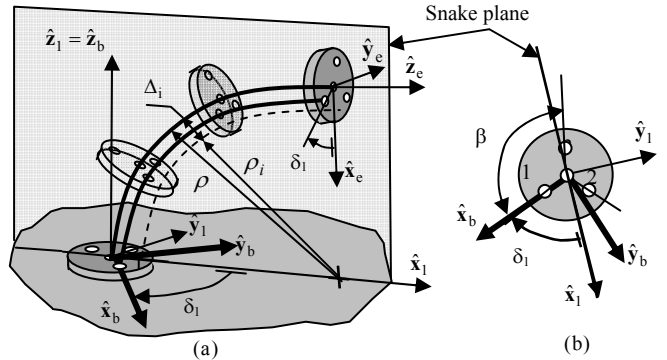


Fig. 4. Kinematic nomenclature used in this paper

- L_d, L_c - Respective lengths of the backbones in the DDU holder and the actuation cone.
- r - Radius of the base, spacer and end disks
- $\rho(s)$ - Radius of curvature of the primary backbone
- $\theta(s)$ - The tilting angle of the primary backbone tangent in the snake plane. $\theta(s = L)$ and $\theta(s = 0)$ are written as θ_L and θ_0 , respectively.
- β - Division angle of the secondary backbones, $\beta = 2\pi/3$
- δ - Right-handed rotation angle of the snake plane in base disk coordinate system
- δ_i - Defined as $\delta_i = \delta + (i - 1)\beta$
- Δ_i - Offset from primary backbone to the projection of the i^{th} secondary backbone on the snake plane.
- \mathbf{J}_{yx} - Jacobian matrix that $\dot{\mathbf{y}} = \mathbf{J}_{yx}\dot{\mathbf{x}}$
- E_{yp}, E_{ys} - Young's modulus for the primary and secondary backbones.

I_p, I_s - Cross-sectional moments of inertia for backbones
 A - Cross-sectional area of the backbones.
 $\boldsymbol{\tau} = [\tau_1, \tau_2, \tau_3]^t$ - Actuation forces on the secondary backbones
 $\tilde{\boldsymbol{\tau}} = [\tilde{\tau}_1, \tilde{\tau}_2, \tilde{\tau}_3]^t$ - Forces from the actuation unit
 μ - Friction coefficient between the backbones and the actuation cone, Fig. 3
 f_i - Friction force on i th secondary backbone, $f_i = \tilde{\tau}_i - \tau_i$
 f_s - Equivalent static friction in the snake cone
Additional numerical values of the snake-like unit parameters are listed in Table I.

TABLE I
NUMERICAL VALUES OF PARAMETERS

$L = 26\text{mm}$	$r = 1.5\text{mm}$	$E_{yp} = E_{ys} = E = 54\text{GPa}$
$d_{op} = d_{os} = d_o = 0.66\text{mm}$	$d_{ip} = d_{is} = d_i = 0.50\text{mm}$	
$L_d = 480\text{mm}$	$L_c = 58\text{mm}$	

The inverse kinematics of the snake-like unit writes:

$$L_i = L + q_i = L + \Delta_i(\theta_L - \theta_0) \quad (1)$$

where $\Delta_i \equiv r \cos(\delta_i)$, $i = 1, 2, 3$. For given q_i , the snake configuration $\boldsymbol{\psi} = [\theta_L, \delta]^t$ is given by:

$$\theta_L = \theta_0 + q_i / \Delta_i \quad (2)$$

$$\delta = \text{atan}2(q_2 - q_1 \cos \beta, -q_1 \sin \beta) \quad (3)$$

The instantaneous direct kinematics is given by:

$$\dot{\boldsymbol{\psi}} = \mathbf{J}_{\boldsymbol{\psi}\mathbf{q}} \dot{\mathbf{q}} \quad (4)$$

Because of the actuation redundancy, there would be only two independent variables among q_1 , q_2 and q_3 . If we pick q_1 and q_2 , the Jacobian matrix $\mathbf{J}_{\boldsymbol{\psi}\mathbf{q}}$ is derived as:

$$\mathbf{J}_{\boldsymbol{\psi}\mathbf{q}} = \begin{bmatrix} \frac{q_2 c_{\delta_1} s_{\delta_1} - q_1 s_{\delta_1 + \delta_2}}{r c_{\delta_1}^2 (q_2 s_{\delta_1} - q_1 s_{\delta_2})} & \frac{q_1 c_{\delta_1} s_{\delta_1}}{r c_{\delta_1}^2 (q_2 s_{\delta_1} - q_1 s_{\delta_2})} \\ -c_{\delta_2} & c_{\delta_1} \\ \frac{q_2 s_{\delta_1} - q_1 s_{\delta_2}}{q_2 s_{\delta_1} - q_1 s_{\delta_2}} & \frac{c_{\delta_1}}{q_2 s_{\delta_1} - q_1 s_{\delta_2}} \end{bmatrix} \quad (5)$$

Where $c_x = \cos x$, $s_x = \sin x$

As shown in Fig 6, when the snake-like unit is bent by the actuation unit, the forces exerted on the secondary backbones expand or compress the flexible backbones in the long DDU holder. The secondary backbones pass through channels in the snake cone, and the frictions in the channels generates additional axial extension/compression on the backbones. Due to actuation errors generated by this extension or compression, the actual configuration of the snake-like unit deviates from its desired configuration. The corrected inverse kinematics is now given by:

$$L_i = L + \Delta_i(\theta_L - \theta_0) + \varepsilon_i(\theta_L, \delta) \quad (6)$$

To obtain rough knowledge about $\varepsilon_i(\theta_L, \delta)$, we can substitute Eq (2) into Eq. (5) and simplify $\mathbf{J}_{\boldsymbol{\psi}\mathbf{q}}$ to:

$$\mathbf{J}_{\boldsymbol{\psi}\mathbf{q}} = \begin{bmatrix} \frac{s_{\delta_2}}{r \sin \beta} & \frac{-s_{\delta_1}}{r \sin \beta} \\ \frac{q_2}{r^2 \theta_L^2 \sin \beta} & \frac{-q_1}{r^2 \theta_L^2 \sin \beta} \end{bmatrix} \quad (7)$$

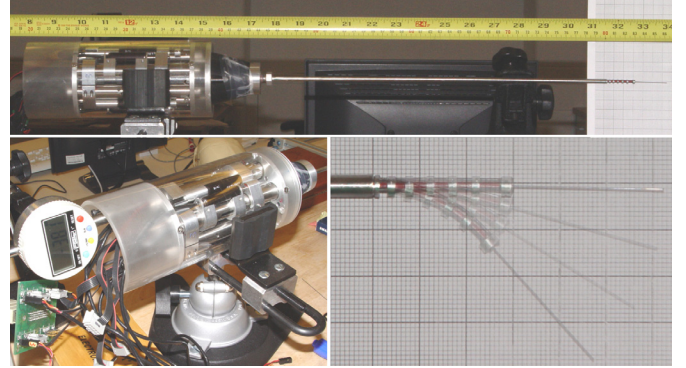


Fig 5. The snake-like unit assembled to its actuation unit (top). Experimental setup used to calibrate the snake-like unit (bottom).

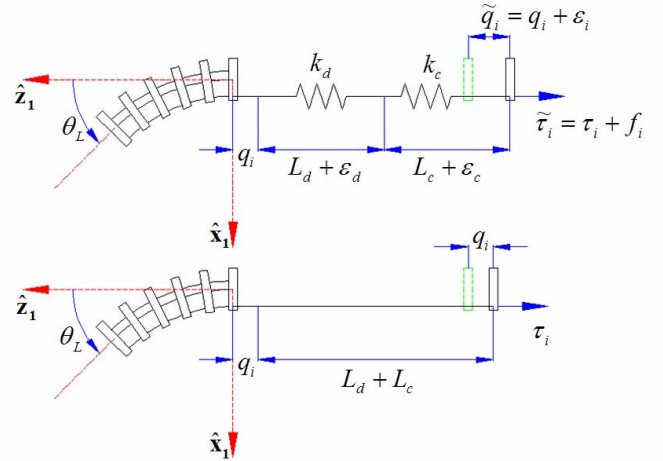


Fig 6. Stiffness compensation model for a snake with extensible backbones (top) and an ideal snake with non-extensible backbones (bottom).

Since $\Delta \boldsymbol{\psi} = \mathbf{J}_{\boldsymbol{\psi}\mathbf{q}} \Delta \mathbf{q}$, from Eq (7), we can conclude:

- 1) When θ_L is small, errors on δ will dominate. However, this would harm less since when θ_L is small, position errors of the snake tip is also relatively small.
- 2) Errors on θ_L will always increase when Δq_i increase, while Δq_i increases as the desired θ_L increases.
- 3) Refer to Fig 6, when θ_L is relative large, Δq_i will always have the same sign with q_i and will be roughly proportional to q_i . Hence, $\Delta \delta = \frac{q_2 \Delta q_1 - q_1 \Delta q_2}{r^2 \theta_L^2 \sin \beta}$ can be very small even

zero. This explains why under some configurations, errors on δ are considerably diminished.

The significant flexibility of the secondary backbones also greatly influences the kinematics of the snake-like unit. The corrected instantaneous kinematics is given by:

$$\dot{\psi} = \tilde{\mathbf{J}}_{\psi\mathbf{q}} \dot{\mathbf{q}} \quad (8)$$

Where $\tilde{\mathbf{J}}_{\psi\mathbf{q}}$ is the corrected Jacobian presented in section VI.

III. MODELS OF ACTUATION FORCE AND FRICTION

As described in section II, there are two main sources of error in the actuation system. Two models are introduced here to calculate the extension/compression on the backbones.

A. Virtual Work of the Snake-Like Unit

Since the length of the snake-like unit (26mm) is much shorter than the length of the DDU holder (480mm), the extension or compression of the backbones within the range of the snake-like unit is negligible. The static model of the snake-like unit given in Eq. (9) was ever addressed in detail by our previous work [21] where \mathbf{w}_e is the wrench applied on the snake-like unit by its environment, $\mathbf{J}_{x\psi}$ is the instantaneous kinematics Jacobian such that $\dot{\mathbf{x}} = \mathbf{J}_{x\psi} \dot{\psi}$, and \mathbf{x} is the 6×1 pose vector defining the position and orientation of the snake-like unit. $\mathbf{J}_{x\psi}$ and $\mathbf{J}_{q\psi}$ were also both given in [21].

$$\mathbf{J}_{q\psi}^t \boldsymbol{\tau} = \nabla \mathbf{E} + \mathbf{J}_{x\psi}^t \mathbf{w}_e \quad (9)$$

With the virtual work equations, an optimization process is introduced. The solution presented here is a simplified special case, with no external wrench on the tip of the snake.

$$\text{Min}_{\boldsymbol{\tau}} Z = \frac{1}{2} (\tau_1^2 + \tau_2^2 + \tau_3^2) = \frac{1}{2} \boldsymbol{\tau}^t \boldsymbol{\tau} \quad (10)$$

$$\text{s.t. } \mathbf{J}_{q\psi}^t \boldsymbol{\tau} = \nabla \mathbf{E}$$

For simplicity and real-time computability, the optimal distribution of load on the secondary backbones is derived as:

$$\boldsymbol{\tau} = \mathbf{J}_{q\psi} (\mathbf{J}_{q\psi}^t \mathbf{J}_{q\psi})^{-1} \nabla \mathbf{E} \quad (11)$$

B. Friction Model

The main source of friction is the actuation cone in Fig 3. The channel of this cone consists of two 41° circular sections with a curvature of 20 mm and a tangential straight portion. According to the model of flat belt brakes [29], the actuation force τ_i on the backbone and the actuation force $\tilde{\tau}_i$ from the actuation unit have the following relationship:

$$\tilde{\tau}_i = \tau_i \cdot e^{2\mu\varphi} \quad (12)$$

We next add to our model a friction component $f_s e^{2\mu\varphi}$ that accounts for the contact forces between the backbones and the cone as the backbones are bent to the shape of the channels, Eq. (13). The efficacy of this model is shown in section VI.

$$\tilde{\tau}_i = (\tau_i + f_s) \cdot e^{2\mu\varphi}, \quad \varphi = 41^\circ \quad (13)$$

A calibration experiment was designed to obtain equivalent static friction force f_s and friction coefficient μ by measuring the relationship between actuation force on the backbone τ_i and the actuation force $\tilde{\tau}_i$ from the actuation unit. The experiment setup is shown in Figs 7, 8. The backbone is inserted into the snake cone and clamped at both

ends. Standard calibration weights are used as forces which act on one end of the backbone. A force scale is used to measure the actuation force. The experiment results are listed in Table II. Least square curve fitting results is: $f_s = 1.959N$ and $\mu = 0.1727$. The curve fitting results are shown in Fig 8.

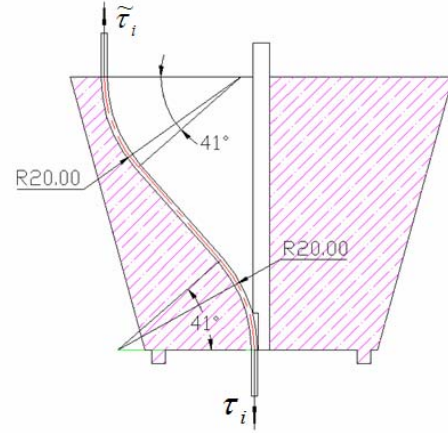


Fig 7. A typical channel in the Snake Cone

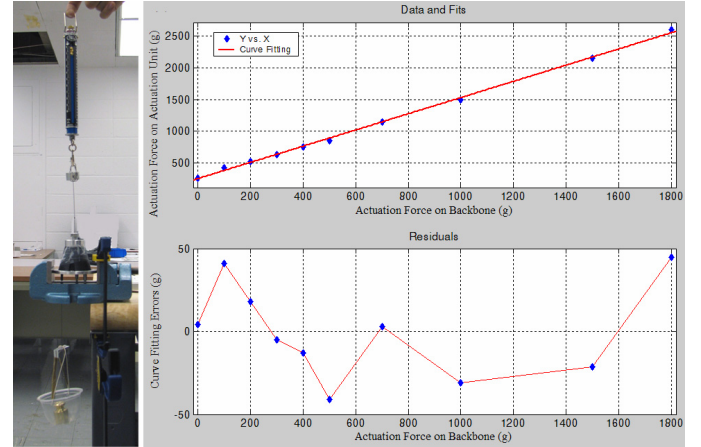


Fig 8. Experiment and Curve Fitting for Friction Calibration

TABLE II
FRICTION CALIBRATION EXPERIMENT RESULTS

τ_i [g]	$\tilde{\tau}_i$ [g]	τ_i [g]	$\tilde{\tau}_i$ [g]
0 ± 1	255 ± 25	100 ± 1	420 ± 25
200 ± 1	525 ± 25	300 ± 1	630 ± 25
400 ± 1	750 ± 25	500 ± 1	850 ± 25
700 ± 1	1150 ± 25	1000 ± 1	1500 ± 25
1500 ± 1	2150 ± 25	1800 ± 1	2600 ± 25

The error limits of the parameter fitting are obtained from Eq (13) by differentiation:

$$\begin{aligned} df_s &= e^{-2\mu\varphi} d\tilde{\tau}_i - d\tau_i = 0.020N \\ d\mu &= \frac{1}{2\varphi} \frac{1}{\tilde{\tau}_i} d(\tilde{\tau}_i) - \frac{1}{2\varphi} \frac{1}{f_s + \tau_i} d\tau_i = 0.0135 \end{aligned} \quad (14)$$

Therefore $f_s = 1.96 \pm 0.020N$ and $\mu = 0.17 \pm 0.014$.

IV. CLOSED FORM NAIVE COMPENSATION

With all the theoretical derivations, we naively introduce the compensation equation (please also refer to Fig 6):

$$\tilde{\mathbf{q}} = \mathbf{q} + \boldsymbol{\varepsilon} \quad (15)$$

The stiffness matrices of the backbone sections in the DDU holder and in the snake cone are \mathbf{K}_d and \mathbf{K}_c , respectively.

$$\boldsymbol{\varepsilon} = \mathbf{K}_d^{-1} \boldsymbol{\tau} + \mathbf{K}_c^{-1} \tilde{\boldsymbol{\tau}} \quad (16)$$

$$\mathbf{K}_d = \begin{bmatrix} E_{ys}A/L_d & & \\ & E_{ys}A/L_d & \\ & & E_{ys}A/L_d \end{bmatrix}, \quad \mathbf{K}_c = \begin{bmatrix} E_{ys}A/L_c & & \\ & E_{ys}A/L_c & \\ & & E_{ys}A/L_c \end{bmatrix} \quad (17)$$

Item $\mathbf{K}_c^{-1} \tilde{\boldsymbol{\tau}}$ in Eq. (16) is actually an approximation, accounting for the integral of varying compression due to varying force along the backbone in the snake cone.

The experimental result with this scheme implemented is shown in Fig 10. The result shows that the bending error has a non-linearity when the desired bending angle is small. When the desired bending angle increases, the bending error shows some linearity again. This phenomenon suggests that the system has some backlash somewhere, which dominates when the desired bending angle is small. And we are missing certain proportional aspect (e.g. friction between the backbones and the spacer disks) of the real prototype, which will dominate when the desired bending angle increases.

An easy measurement supports our postulate. In Fig 5, a dial indicator is inserted into the actuation unit to measure the real displacement of the actuation unit. The measurement shows a 0.15-0.20 mm backlash in the actuation unit. We next present a recursive compensation scheme.

V. COMPENSATION BASED ON RECURSIVE ESTIMATION

We chose a recursive linear estimation approach [30] to improve our actuation compensation and to support real-time computing. We assume that the configuration of the snake-like unit $\boldsymbol{\psi} = [\theta_L, \delta]^t$ can be measured by external means (e.g. robot vision). We account for backlash in the actuation unit and friction in the snake-like unit by introducing two new parameters η and $\boldsymbol{\lambda} = [\lambda, \lambda, \lambda]^t$. The scalar η is a scaling factor for the snake actuation forces $\boldsymbol{\tau}$. It accounts for friction and deviation of the real snake-like unit from an ideal snake-like unit due to the fact that the spacer disks have a finite thickness that affects the bending of the snake (due to stress concentrations). The vector $\boldsymbol{\lambda}$ accounts for backlash in the actuation unit. We assume uniform backlash in all identical actuators. The compensation is now given by:

$$\boldsymbol{\varepsilon} = \eta \mathbf{K}_d^{-1} \boldsymbol{\tau} + \mathbf{K}_c^{-1} \tilde{\boldsymbol{\tau}} + \boldsymbol{\lambda} = \eta \mathbf{K}_d^{-1} \boldsymbol{\tau} + e^{2\mu\phi} \mathbf{K}_c^{-1} (\eta \boldsymbol{\tau} + \mathbf{f}_s) + \boldsymbol{\lambda} \quad (18)$$

Where $\mathbf{f}_s = [f_s, f_s, f_s]^t$. Since μ and f_s are given by our experiments in section III, we will estimate η and $\boldsymbol{\lambda}$. The initial estimation is calculated according to the first two measurements of $\boldsymbol{\varepsilon}$. The observed required compensation, $\boldsymbol{\varepsilon} = \tilde{\mathbf{q}} - \mathbf{q}$, is found by reading $\tilde{\mathbf{q}}$ from the encoders of the actuation unit; while \mathbf{q} is calculated from the inverse kinematics using Eq. (1), and the measured configuration $\boldsymbol{\psi} = [\theta_L, \delta]^t$. As new measurements of $\boldsymbol{\varepsilon}$ are obtained (at this

time, through external measurements, the recursively estimated control parameters are updated manually. We plan to update these measurements automatically through computer vision.), the estimate $\hat{\mathbf{x}} = [\hat{\eta}, \hat{\boldsymbol{\lambda}}]^t$ is updated using:

$$\begin{aligned} \hat{\mathbf{x}}_{k+1} &= \hat{\mathbf{x}}_k + \mathbf{S}_{k+1} (\mathbf{z}_{k+1} - \mathbf{H}_{k+1} \hat{\mathbf{x}}_k) \\ \mathbf{S}_{k+1} &= \mathbf{P}_k \mathbf{H}_{k+1}^t (\mathbf{I} + \mathbf{H}_{k+1} \mathbf{P}_k \mathbf{H}_{k+1}^t)^{-1} \\ \mathbf{P}_k &= (\mathbf{H}_k^t \mathbf{H}_k)^{-1} \end{aligned} \quad (19)$$

where \mathbf{H}_k and \mathbf{z}_k are respectively the k^{th} measurement matrix and the k^{th} measurement of $\boldsymbol{\varepsilon}$, Eq. (19). $\hat{\mathbf{x}}_k = [\hat{\eta}_k, \hat{\boldsymbol{\lambda}}_k]^t$ is the current estimated vector. In Eq.20 $\boldsymbol{\tau}_k$ is calculated based on the redundancy resolution of Eq. (11). The variance of the estimation error is given by Eq. (21) where $\mathbf{K} = (\mathbf{H}^t \mathbf{H})^{-1} \mathbf{H}^t$ and \mathbf{V}_v is the variance of the measurement noise. In our calculations we use the conservative measurement noise standard deviation $\sigma = 1^\circ$ and variance of $\mathbf{V}_v = \sigma^2 \mathbf{I}$, although our measurements have about 0.5° repeatability. The standard deviation of the measurement noise is equivalent to 0.0294mm on $\boldsymbol{\varepsilon}$. The results of the estimation after 10 measurements are shown in table III and given in Eq. (22).

$$\begin{aligned} \mathbf{z}_k &= \begin{bmatrix} \boldsymbol{\varepsilon}_1^t - e^{2\mu\phi} \mathbf{f}_s^t \\ \vdots \\ \boldsymbol{\varepsilon}_k^t - e^{2\mu\phi} \mathbf{f}_s^t \end{bmatrix}, \quad \mathbf{H}_k = \begin{bmatrix} (\mathbf{K}_d \boldsymbol{\tau}_1^t + e^{2\mu\phi} \mathbf{K}_c \boldsymbol{\tau}_1^t) & 1 \\ \vdots & \vdots \\ (\mathbf{K}_d \boldsymbol{\tau}_k^t + e^{2\mu\phi} \mathbf{K}_c \boldsymbol{\tau}_k^t) & 1 \end{bmatrix} \\ \boldsymbol{\zeta} &= \mathbf{K} \mathbf{V}_v \mathbf{K}^t \end{aligned} \quad (20)$$

$$\hat{\eta} = 1.220 \pm 0.0019, \quad \hat{\boldsymbol{\lambda}} = 0.1778 \pm 0.0005 \text{ mm} \quad (22)$$

As a generalization of this approach, if we obtain μ , f_s and $\boldsymbol{\lambda}$ from experiments characterizing the snake, we can estimate the total bending angle ϕ , which would be very useful for applications implementing a flexible actuation stem in minimally invasive surgery. In this case the recursive linear estimation will be updated to include fading memory to account for variations of the friction in the flexible actuation stem as it changes its geometry [30].

Given the estimated parameters, the final compensation is given in Eq. (23) and $\boldsymbol{\varepsilon}$ is given by Eq. (18).

$$\tilde{\mathbf{q}} = \mathbf{q} + \boldsymbol{\varepsilon} \quad (23)$$

The updated instantaneous kinematics of the snake-like unit with compensation has a different Jacobian $\tilde{\mathbf{J}}_{\boldsymbol{\psi}\mathbf{q}}$ that is derived here. For ideal snake with no extensions in its actuation lines the kinematics is given in Eq. (24). By calculating the time derivative of the required compensation in Eq. (25) we find the updated instantaneous kinematics Jacobian according to Eq. (26). The detailed expression for $\boldsymbol{\alpha}(\boldsymbol{\psi})$ remains to be defined in a separate future study.

$$\dot{\boldsymbol{\psi}} = \mathbf{J}_{\boldsymbol{\psi}\mathbf{q}} \dot{\mathbf{q}} = \mathbf{J}_{\boldsymbol{\psi}\mathbf{q}} (\dot{\tilde{\mathbf{q}}} - \dot{\boldsymbol{\varepsilon}}) \quad (24)$$

$$\dot{\mathbf{e}} = \boldsymbol{\eta} \mathbf{K}_d^{-1} \dot{\boldsymbol{\tau}} + \mathbf{e}^{2\mu\phi} \boldsymbol{\eta} \mathbf{K}_c^{-1} \dot{\boldsymbol{\tau}} = \boldsymbol{\alpha}(\boldsymbol{\psi}) \dot{\boldsymbol{\psi}} \quad (25)$$

$$\dot{\boldsymbol{\psi}} = (\mathbf{I} + \mathbf{J}_{\boldsymbol{\psi}q} \boldsymbol{\alpha})^{-1} \mathbf{J}_{\boldsymbol{\psi}q} \dot{\mathbf{q}} \Rightarrow \tilde{\mathbf{J}}_{\boldsymbol{\psi}q} = (\mathbf{I} + \mathbf{J}_{\boldsymbol{\psi}q} \boldsymbol{\alpha})^{-1} \mathbf{J}_{\boldsymbol{\psi}q} \quad (26)$$

VI. SIMULATION AND EXPERIMENTS RESULTS

We conducted both simulations and real bending experiments to validate our models. Figure 9 shows the data of secondary backbone 1 only, since all backbones are subject to the same compensation procedure. Sample experimental results are shown in Fig 10 and Fig 11. The bending angle is measured according to the thin grids on the graph paper in the picture we took. Although the data presented in Figs. 10, 11 is for $\delta = 0^\circ$ and $\theta_L = 30^\circ$, equally good results were obtained for different values of δ and θ_L . Fig 12 shows the bending snake-like unit in several measured configurations.

The experimental data shown in Fig 10 shows that the naive estimation failed to achieve our goal accuracy of 1° . After implementing the combined model-based linear estimation, we achieved the desired accuracy. The results of the recursive estimation process are listed in Table III.

The capability of precisely tracking trajectory is a crucial step towards the successful suturing in a very confined space.

TABLE III
RECURSIVE ESTIMATION

No.	$\hat{\boldsymbol{\eta}}$	$\hat{\boldsymbol{\lambda}}$ (mm)
1	1.5240	0.1194
2	1.6564	0.1085
3	1.5666	0.1191
4	1.4359	0.1394
5	1.2689	0.1723
6	1.2453	0.1777
7	1.2480	0.1770
8	1.2209	0.1853
9	1.2198	0.1778
10	1.2210	0.1765

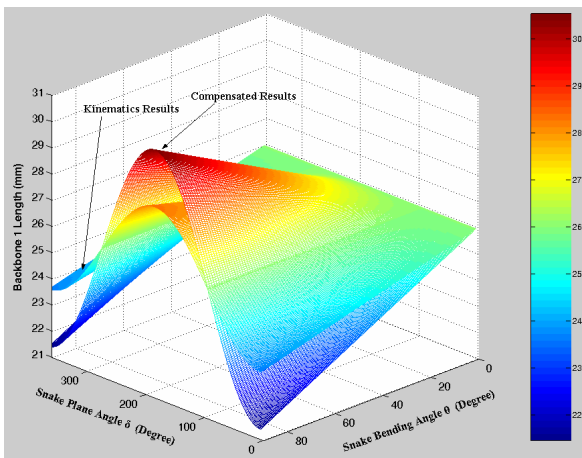


Fig 9. Compensated Length of Backbone 1 over the whole workspace

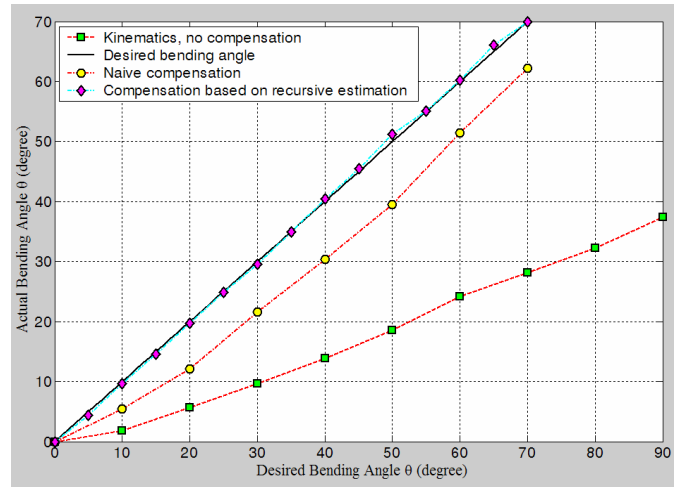


Fig 10. Results of bending experiments for $\delta=0^\circ$ and varying θ

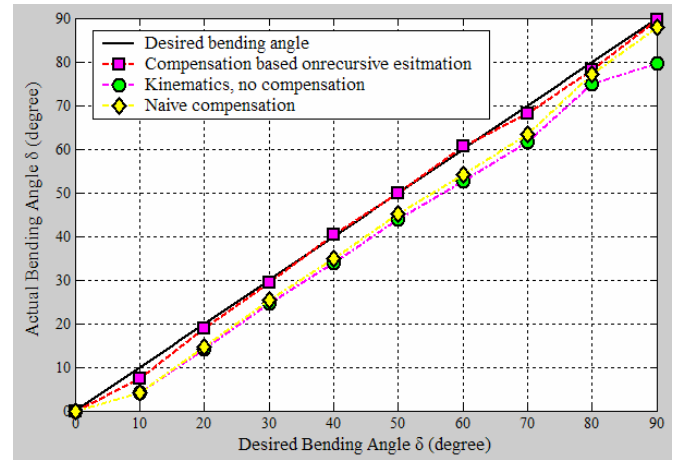


Fig 11. Results of bending experiments for $\theta=30^\circ$ and varying δ

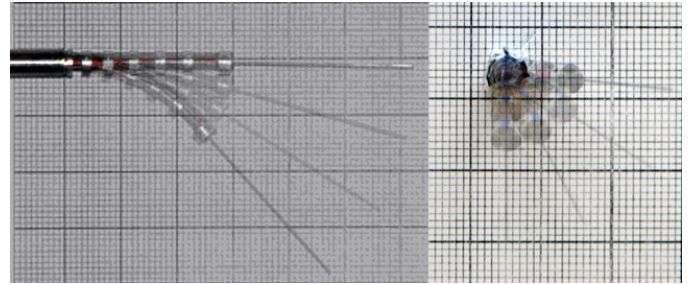


Fig 12. Photographs of the Bending Snake

VII. CONCLUSION

The paper presented a snake-like unit that implements super-elastic backbones as elements of actuation. This design, although has significant advantages in supporting miniaturization and reducing backlash, suffers from modeling and control difficulties due to the flexibility of the actuation lines. The paper presented the static model of this snake-like unit and compared two alternative methods of actuation compensation. The effectiveness of these compensation methods was evaluated in simulations and experiments on our current prototype. The errors in path tracking were significantly reduced by the naive model-based compensation

presented in this paper. However, since the results failed to provide the desired accuracy of about 1° , we implemented a combined model-based linear estimation method to account for inaccuracies in the snake-like unit and backlash in the actuation unit. This method relies on online measurements of the configuration of the snake-like unit to update its Jacobian. The results of this approach achieved the desired accuracy of 1° in bending angle of the snake-like unit. Finally, we presented an updated Jacobian that accounts for the flexibility in the actuation lines. We also showed how to use the compensation model of this paper to compensate for varying friction in robots that use flexible actuation stems.

ACKNOWLEDGEMENT

This work was partially funded by the National Science Foundation (NSF) under Engineering Research Center grant #EEC9731478, NSF grant #IIS9801684, and by the National Institutes of Health (NIH) under grant #R21 EB004457-01 and by Columbia University and Johns Hopkins University internal funds.

REFERENCES

- [1] S. Charles, "Dexterity enhancement for surgery," R. H. Taylor, S. Lavallee, G. C. Burdea, and R. Mosges, Eds. Cambridge, MA: MIT Press, 1996, pp. 467-472.
- [2] R. Taylor, J. Funda, B. Eldridge, S. Gomory, K. Gurben, D. LaRose, et al., "A telerobotics assistant for laparoscopic surgery," *IEEE Engineering in Medicine and Biology Magazine*, vol. 14, pp. 279-288, 1995.
- [3] N. Simaan, R. Taylor, and P. Flint, "A dexterous system for laryngeal surgery - multi-backbone bending snake-like slaves for teleoperated dexterous surgical tool manipulation," in *IEEE International Conference on Robotics and Automation*. New Orleans, 2004, pp. 351-357.
- [4] M. Minor and R. Mukherejee, "A dexterous manipulator for minimally invasive surgery," in *IEEE International Conference on Robotics and Automation*, 1999, pp. 2057-2064.
- [5] H. Yamashita, D. Kim, N. Hata, and T. Dohi, "Multi-slider linkage mechanism for endoscopic forceps manipulator," in *IEEE International Conference on Intelligent Robots and Systems (IROS)*, vol. 3, 2003, pp. 2577-2582.
- [6] J.-P. Merlet, "Optimal design for the micro parallel robot mips," in *IEEE International Conference on Robotics and Automation*, vol. 2, 2002, pp. 1149-1154.
- [7] C. Reboulet and S. Durand-Leguay, "Optimal design of redundant parallel mechanism for endoscopic surgery," in *IEEE International Conference on Intelligent Robots and Systems*, vol. 3, 1999, pp. 1432-1437.
- [8] D. Asai, S. Katopo, J. Arata, S. i. Warisawa, M. Mitsuishi, A. Morita, et al., "Micro-neurosurgical system in the deep surgical field," in *MICCAI 2004 (7th International Conference on Medical Image Computing and Computer-Assisted Intervention)*, vol. LNCS 3217, 2004, pp. 33-40.
- [9] A. J. Madhani, G. Niemeyer, and K. Salisbury, "The black falcon: A teleoperated surgical instrument for minimally invasive surgery," in *IEEE/RSJ International Conference on Intelligent Robots and Systems (IROS)*, 1998, pp. 936-944.
- [10] P. S. Schenker, E. C. Barlow, C. D. Boswell, H. Das, S. Lee, T. R. Ohm, et al., "Development of a telemanipulator for dexterity enhanced microsurgery," in *2nd Annual International Symposium on Medical Robotics and Computer Assisted Surgery (MRCAS)*, 1995, pp. 81-88.
- [11] P. Dario, M. C. Carrozza, A. Pietrabissa, and C. A. Surgery, "Development and in vitro testing of a miniature robotic system for computer-assisted endoscopy," vol. 4, pp. 1-14, 1999.
- [12] P. Dario, C. Paggetti, N. Troisfontaine, E. Papa, T. Ciucci, M. C. Carrozza, et al., "A miniature steerable end-effector for application in an integrated system for computer-assisted arthroscopy," in *IEEE International Conference on Robotics and Automation*, 1997, pp. 1573-1579.
- [13] K. Harada, K. Tsubouchi, M. G. Fujie, and T. Chiba, "Micro manipulators for intrauterine fetal surgery in an open mri," in *IEEE International Conference on Robotics and Automation*, 2005, pp. 504-509.
- [14] K. Ikuta, K. Yamamoto, and K. Sasaki, "Development of remote microsurgery robot and new surgical procedure for deep and narrow space," in *IEEE International Conference on Robotics and Automation*, 2003, pp. 1103-1108.
- [15] J. Piers, D. Reynaerts, and H. V. Brussel, "Design of miniature parallel manipulators for integration in a self-propelling endoscope," *Sensors and Actuators*, vol. 85, pp. 409-417, 2000.
- [16] D. Reynaerts, J. Peirs, and H. Van Brussel, "Shape memory micro-actuation for a gastro-intestinal intervention system," *Sensors and Actuators*, vol. 77, pp. 157-166, 1999.
- [17] H. Yamashita, N. Hata, M. Hashizume, and T. Dohi, "Handheld laparoscopic forceps manipulator using multi-slider linkage mechanisms," in *MICCAI 2004 (7th International Conference on Medical Image Computing and Computer-Assisted Intervention)*, vol. LNCS 3217, 2004, pp. 121-128.
- [18] M. Mitsuishi, H. Watanabe, H. Nakanishi, H. Kubota, and Y. IIZUKA, "Dexterity enhancement for a tele-micro-surgery system with multiple macro-micro co-located operation point manipulators and understanding of the operator's intention," in *Lecture notes in computer science (lncs)*, vol. 1205, J. Troccaz, E. Grimson, and R. Mosges, Eds.: Springer, 1997, pp. 821-830.
- [19] A. Kapoor, N. Simaan, and R. Taylor, "Suturing in confined spaces: Constrained motion control of a hybrid 8-dof robot"; international conference on advanced robotics," *International Conference on Advanced Robotics (IACR'2005)*, 2005.
- [20] N. Simaan, "High dexterity snake-like robotic slaves for minimally invasive telesurgery of the upper airway," in *MICCAI 2004 (7th International Conference on Medical Image Computing and Computer-Assisted Intervention)*, vol. LNCS 3217, C. Barillot, D. R. Haynor, and P. Hillier, Eds., 2004, pp. 17-24.
- [21] N. Simaan, "Snake-like units using flexible backbones and actuation redundancy for enhanced miniaturization," in *IEEE International Conference on Robotics and Automation*. Barcelona, Spain, 2005, pp. In press.
- [22] I. Gravagne and I. Walker, "On the kinematics of remotely-actuated continuum robots," in *IEEE International Conference on Robotics and Automation*, 2000, pp. 2544-2550.
- [23] I. A. Gravagne and I. D. Walker, "Manipulability, force and compliance analysis for planar continuum manipulators," *IEEE Transaction of Robotics and Automation*, vol. 18, pp. 263-273, 2002.
- [24] M. A. Meggiolaro and S. Dubowsky, "An analytical method to eliminate the redundant parameters in robot calibration," in *IEEE International Conference on Robotics and Automation*. San Francisco, CA, USA, 2000.
- [25] M. M. Svinin and M. Uchiyama, "A new compensation scheme for the inverse kinematics tasks of flexible robot arms," in *IEEE International Conference on Robotics and Automation*, vol. Volume 1. San Diego, CA, USA: IEEE Computer Society Press, 1994.
- [26] D. W. Williams and D. A. Turcic, "An inverse kinematic analysis procedure for flexible open-loop mechanisms," *Journal of Mechanism and Machine Theory*, vol. 27, pp. 701-714, 1992.
- [27] G. Chirikjian and J. Burdick, "Kinematically optimal hyper-redundant manipulator configurations," *IEEE Transactions on Robotics and Automation*, vol. 11, pp. 794-806, 1995.
- [28] K. Zanganeh and J. Angeles, "The inverse kinematics of hyper-redundant manipulators using splines," in *IEEE International Conference on Robotics and Automation*, 1995, pp. 2797-2802.
- [29] R. C. Juvinall and K. M. Marshek, *Fundamentals of machine component design*, 3rd ed: John Wiley & Sons, Inc, 2000.
- [30] A. P. Sage and J. L. Melsa, *Estimation theory with application to communications and control*: McGraw-Hill Book Company, 1971.